Sixth International Symposium on Turbulence and Shear Flow Phenomena
Seoul, Korea, 22-24 June 2009

OPTIMAL AMPLIFICATION OF LARGE-SCALE STRUCTURES IN PLANE TURBULENT COUETTE FLOW

Yongyun Hwang
Laboratorie d'hydrodynamique (LadHyX),
École Polytechnqiue, F-91128 Palaiseau, France
yongyun.hwang@ladhyx.polytechnique.fr

Carlo Cossu
Laboratorie d'hydrodynamique (LadHyX),
CNRS-École Polytechnqiue, F-91128 Palaiseau, France
carlo.cossu@ladhyx.polytechnique.fr

ABSTRACT

In the present study, we investigate the optimal perturbations in plane turbulent Couette flow with turbulent mean flow and the associated eddy viscosity at $Re_h = 750$. The three canonical types of optimal perturbations are computed: the initial perturbations for transient energy growth, the response to harmonic forcing and the variance to stochastic excitation. In all the cases, the maximum responses are obtained for streamwise uniform perturbations ($\lambda_x = \infty$). The optimal spanwise spacings of the transient growth and the stochastic forcing are $\lambda_z = 4.2h$ and $\lambda_z = 5.2h$, respectively. These values are in very good agreement with the spanwise spacing of the large-scale streaks reported in previous studies. Moreover, the velocity field of the responses to the optimal perturbations are strikingly similar to that of large-scale structure obtained with direct numerical simulation. Finally, the optimal response to the harmonic forcing, more related to flow controls, reveals the maximum by steady forcing with larger spanwise wavelength ($7.4h$).

INTRODUCTION

The fully developed turbulent plane Couette flow is one of the first canonical cases in which very large coherent and persistent streaky structures have been observed. Lee & Kim (1991) observed structures elongated in the streamwise direction with a roughly circular cross-section in their direct numerical simulation of the fully developed turbulent Couette flow. In order to understand if the spanwise size of these large scale structures was the largest possible, Komminaho *et al.* (1996) repeated the simulations at $Re_h = 750$ using a huge computational box ($L_x \times L_y \times L_z = 28\pi \times 2 \times 8\pi$). They found that the most probable spanwise spacing of these vortical structures is about $4h$ where h is the half height of channel and that these structures can be suppressed by rotation around the spanwise axis. Very recently, Kitoh *et al.* (2005) and Kitoh & Umeki (2008) experimentally studied these structures at $Re_h = 3750$ and found typical spanwise wavelengths of the order of $4 \sim 5h$.

At the same time similar large scale structures were found in direct numerical simulations and experiments in the plane pressure driven channel flow and in the turbulent boundary layer. Recent investigations (del Álamo & Jiménez 2006; Cossu *et al.* 2009; Pujals *et al.* 2009) have revealed a possible connection between the observed large scale structures and the optimal perturbations of the turbulent mean flows. In all these studies, analytical expressions that matched the mean velocity profiles and the turbulent eddy viscosity, were used to compute the optimal perturbations leading to the maximum transient growth. It was found that there are two local peaks in maximum transient growth with respect to the spanwise spacing. The first peak scales well with respect to outer length scale h and the spanwise spacing for maximum response showed good agreement with that of large-scale streaky structures in the outer layer. The secondary peak scales well with respect to the inner length scale ν/u_τ where ν and u_τ are kinematic viscosity and friction velocity, respectively. This secondary peak corresponds to the $\lambda_z^+ \approx 100$ typical of streaks in the inner layer.

No investigation of the optimal energy amplifications sustained by the turbulent Couette are currently available, even if the presence of large-scale coherent streaks with the spanwise spacing of $4 - 5h$ is a well-established feature of this flow. Furthermore, del Álamo & Jiménez (2006), Cossu *et al.* (2009) and Pujals *et al.* (2009) have only considered the optimal temporal energy growth whereas the optimal responses to harmonic and stochastic forcing may be equally relevant and their computation for laminar flows have been extensively computed: e.g. Farrell & Ionnou (1993), Jovanović & Bamieh (2005) and so on. In this respect, some relevant questions are still opened: What are the streamwise and spanwise spacings amplified most by the initial perturbation, the harmonic forcing, and stochastic excitation in the turbulent Couette flow ? How do they compare among them and with analogous results found in laminar flows? What are the spatial structures of the corresponding optimal perturbations? How do these structures relate to the large-scale coherent streaks observed in experiments and direct numerical simulations? Do their spanwise spacing relate well to coherent as found in the turbulent Poiseulle flow, or are they larger as found in the turbulent boundary layer?

In order to answer to these questions, we have conducted an input-output analysis with the mean velocity profile of turbulent Couette flow by considering its optimal responses to initial perturbation, harmonic forcing, and stochastic excitation. In the last case, the more correlated structures (the Karhunen-Loève modes) have also been computed.

BACKGROUND

Turbulent mean flow and eddy viscosity

We consider the plane Couette flow of a viscous fluid of kinematic viscosity ν and constant density ρ between two parallel plates located at $y = \pm h$, where we denote by x, y and z the streamwise, wall-normal and spanwise coordinates respectively. The plates move in opposite directions with velocity $(\pm U_w, 0, 0)$. For sufficiently high values of the Reynolds number $Re = hU_w/\nu$, the flow is turbulent. No analytic approximation of the turbulent mean flow and/or of the associated eddy viscosity is currently available for the turbulent Couette flow contrary to the turbulent Poiseulle flow and boundary layer. We have therefore computed the turbulent mean flow using direct numerical simulation. Once that $U(y)$ is known, it is straightforward to compute the mean shear stress at the wall $\tau_w/\rho = \nu dU/dy|_w$, the friction velocity $u_\tau = \sqrt{\tau_w/\rho}$ and the friction Reynolds number $Re_\tau = u_\tau h/\nu$. Since the mean pressure gradient is zero in the Couette flow, the mean shear stress $\tau = -\rho\overline{u'v'} + \rho\nu dU/dy$ (where u' and v' are the streamwise and the wall-normal velocity fluctuations, respectively) is constant and equal to its value at the wall τ_w. By introducing the eddy viscosity $\nu_t(y) = -\overline{u'v'}/(dU/dy)$, it is found that:

$$\left[\frac{\nu_t(y)}{\nu} + 1\right] \frac{d(U/u_\tau)}{d(y/h)} = Re_\tau. \tag{1}$$

The (total) effective viscosity is then defined as $\nu_T = \nu_t + \nu$.

Generalised Orr-Sommerfeld-Squire equations

Following the approach of Reynolds & Hussain (1972), del Álamo & Jiménez (2006), Cossu *et al.* (2009) and Pujals *et al.* (2009), we consider the linearised equations satisfied by small coherent perturbations in the presence of the associated effective viscosity $\nu_T(y)$. The streamwise and spanwise homogeneity of the problem allow to consider separately each in-plane Fourier mode $\hat{\mathbf{u}}(y,t;\alpha,\beta)e^{i(\alpha x+\beta z)}$ and $\hat{\mathbf{f}}(y,t;\alpha,\beta)e^{i(\alpha x+\beta z)}$, where α and β are the streamwise and spanwise wavenumbers respectively. Then, the following generalised Orr-Sommerfeld-Squire system is obtained as

$$\frac{\partial}{\partial t}\begin{bmatrix}\hat{v}\\ \hat{\eta}\end{bmatrix} = \underbrace{\begin{bmatrix}\Delta^{-1}\mathcal{L}_{\mathcal{OS}} & 0\\ -i\beta U' & \mathcal{L}_{\mathcal{SQ}}\end{bmatrix}}_{\mathbf{A}}\begin{bmatrix}\hat{v}\\ \hat{\eta}\end{bmatrix} + \underbrace{\begin{bmatrix}-i\alpha\Delta^{-1}\mathcal{D} & -k^2\Delta^{-1} & -i\beta\Delta^{-1}\mathcal{D}\\ i\beta & 0 & -i\alpha\end{bmatrix}}_{\mathbf{B}}\begin{bmatrix}\hat{f_u}\\ \hat{f_v}\\ \hat{f_w}\end{bmatrix} \tag{2}$$

with the generalised Orr-Sommerfeld and Squire operators,

$$\begin{aligned}\mathcal{L}_{\mathcal{OS}} &= -i\alpha(U\Delta - U'') + \nu_T\Delta^2 + 2\nu_T'\Delta\mathcal{D}\\ &\quad +\nu_T''(\mathcal{D}^2 + k^2),\\ \mathcal{L}_{\mathcal{SQ}} &= -i\alpha U + \nu_T\Delta + \nu_T'\mathcal{D}.\end{aligned} \tag{3}$$

Here, $\mathcal{D}$ and $'$ denote $\partial/\partial y$, $\Delta = \mathcal{D}^2 - k^2$, $k^2 = \alpha^2 + \beta^2$, and $\hat{\eta}$ is the wall-normal vorticity Fourier mode. The system is completed by the initial condition $\hat{\mathbf{u}}|_{t=0} = \hat{\mathbf{u}}_\mathbf{0}$ and homogeneous boundary conditions for the velocity perturbations on the walls, which result in $\hat{v}(y = \pm h) = 0$, $\mathcal{D}\hat{v}(\pm h) = 0$ and $\hat{\eta}(\pm h) = 0$. The velocity components can be retrieved from the wall-normal variables with:

$$\begin{bmatrix}\hat{u}\\ \hat{v}\\ \hat{w}\end{bmatrix} = \underbrace{\frac{1}{k^2}\begin{bmatrix}i\alpha\mathcal{D} & -i\beta\\ k^2 & 0\\ i\beta\mathcal{D} & i\alpha\end{bmatrix}}_{\mathbf{C}}\begin{bmatrix}\hat{v}\\ \hat{\eta}\end{bmatrix}. \tag{4}$$

Optimal perturbations

We consider the optimal response of the system (4) to initial conditions, harmonic forcing and stochastic forcing. The definition of these optimals is briefly recalled below. The optimal temporal energy growth of (α,β) modes is found by optimizing over the shape of the initial condition the ratio of the energy of the response at a given time t to the energy of the initial condition: $G(t;\alpha,\beta) \equiv \max_{\hat{\mathbf{u}}_0\neq\mathbf{0}} \|\hat{\mathbf{u}}(t;\alpha,\beta)\|^2/\|\hat{\mathbf{u}}_0(\alpha,\beta)\|^2$, where $\|\hat{\mathbf{u}}\|^2 = \int_\Omega |\hat{u}|^2 + |\hat{v}|^2 + |\hat{w}|^2 d\Omega$ and $\Omega = [0, 2\pi/\alpha] \times [-h, h] \times [0, 2\pi/\beta]$. The maximum growth is defined by further maximizing in time $G_{\max}(\alpha,\beta) \equiv \max_t G(t;\alpha,\beta)$ and it is attained at $t = t_{max}$.

When harmonic forcing $\hat{\mathbf{f}}(y,t) = \tilde{\mathbf{f}}(y)e^{-i\omega_f t}$ is applied with frequency ω_f, the response $\hat{\mathbf{u}}(y,t) = \tilde{\mathbf{u}}(y)e^{-i\omega_f t}$ is observed after the switch-on transients have decayed, assuming that the system is stable. In this case, the optimal response is the one having the maximum ratio of the energy of the response to the energy of the forcing: $R(\omega_f;\alpha,\beta) = \max_{\tilde{\mathbf{f}}\neq\mathbf{0}} \|\tilde{\mathbf{u}}(\omega_f;\alpha,\beta)\|^2/\|\tilde{\mathbf{f}}(\omega_f;\alpha,\beta)\|^2$. The optimal response $R(\omega_f)$ is given by the norm of the resolvent operator along the imaginary axis $\zeta = -i\omega_f$. The maximum response $R_{\max}(\alpha,\beta) = \max_{\omega_f} R(\omega_f;\alpha,\beta)$ is obtained with $\omega_{f,\max}$, and is also referred to as H_∞-norm of the transfer function relating the forcing to the response (Zhou *et al.* 2009).

The response to the stochastic forcing $\hat{\mathbf{f}}(t,y)\, e^{i(\alpha x+\beta z)}$ with Gaussian probability distribution and zero mean value $\langle\hat{\mathbf{f}}\rangle = \mathbf{0}$ is finally considered. The forcing is assumed to be delta-correlated in time: $\langle\hat{\mathbf{f}}(y,t)\otimes\hat{\mathbf{f}}^*(y',t')\rangle = \mathbf{R}\delta(t-t')$ where * denotes complex conjugation and $\delta(t)$ is the Dirac's delta function. We also assume, without loss of generality, that $\mathbf{R} = \mathbf{I}$. The variance of the response, $V(\alpha,\beta) = \langle\hat{\mathbf{u}}\cdot\hat{\mathbf{u}}^*\rangle$, also referred to as H_2-norm of the transfer function relating the forcing to the output (Zhou *et al.* 2009), is given by: $V(\alpha,\beta) = trace(\mathbf{C}\mathbf{X}_\infty\mathbf{C}^\dagger)$, where the superscript † denotes the adjoint operator with respect to the standard inner product $(\mathbf{h},\mathbf{g}) = \int_\Omega \mathbf{g}^*\cdot\mathbf{h}\, d\Omega$ and $\mathbf{X}_\infty$ is the solution of the following algebraic Lyapunov equation:

$$\mathbf{A}\mathbf{X}_\infty + \mathbf{X}_\infty\mathbf{A}^\dagger + \mathbf{B}\mathbf{B}^\dagger = 0. \tag{5}$$

Since $\mathbf{C}\mathbf{X}_\infty\mathbf{C}^\dagger$ is Hermitian, it has real eigenvalues σ_j and a set of mutually orthogonal eigenfunctions that are usually referred to as 'empirical orthogonal functions' (EOF) or Karhunen-Loève (KL) or 'proper orthogonal decomposition' (POD) modes. The variance being $V = \sum\sigma_j$, the ratio σ_j/V represents the contribution of the j-th mode to the (total) variance. The mode corresponding to the largest σ_j is the optimal one in the sense that it contributes most to the total variance of the system. The part of the stochastic forcing accounting for that optimal mode is computed by solving the dual Lyapunov problem. For further details, the interested reader is referred to the papers by Farrell & Ionnou (1993), Jovanović & Bamieh (2005), and so on.

Numerical tools

The direct numerical simulation of the turbulent channel flow, necessary compute the mean flow, has been performed using the `channelflow` code (Gibson *et al.* 2008) that integrates the incompressible Navier-Stokes equation using a spectral method based on the Fourier-Galerkin discretization in the streamwise and spanwise directions, and the Chebyshev-tau discretization in the wall-normal direction. The solution is advanced in time using a third-order semi-implicit time-stepping. Dealiasing with the 2/3 rule is implemented in the streamwise and spanwise directions.

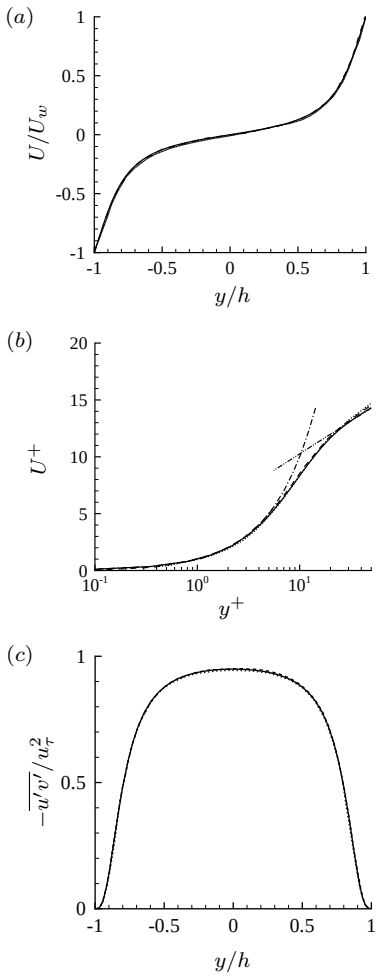

Figure 1: Turbulent mean velocity profile and shear stress from direct numerical simulations. (a) Mean velocity profile expressed in outer units, (b) Same profile expressed in inner units $U^+ \equiv (U + U_w)/u_\tau$ and $y^+ = (y + h)u_\tau/\nu$ and compared to the curves $U^+ = y^+$ (——·——·——) and $U^+ = (1/0.4)\ \log\ y^+ + 4.5$ (——··——··——), (c) Turbulent mean shear stress $-\overline{u'v'}/{u_\tau}^2$. Here, the present DNS (———), Komminaho *et al.* (1996) (– – – –) and Tsukahara *et al.* (2006) (·····); the curves are almost undistinguishable.

The generalised Orr-Sommerfeld-Squire system (4) is discretized using a Chebyshev-collocation method with N_y collocation points in the wall-normal direction. The differentiation operators are discretized using the Chebyshev differentiation matrices of that include the appropriate boundary conditions for $\hat{v}$ and $\hat{\eta}$. The optimal transient growth and the optimal harmonic response are computed using standard methods described. The Lyapunov equation (5), discretized by the same method, was solved using the `lyap` function in `matlab`. The algorithms used to compute the optimal harmonic and stochastic responses have been validated by comparing the results obtained for laminar Couette and Poiseulle flows with those of Schmid & Henningson (2001) and Jovanović & Bamieh (2005). The results in the present study are obtained with $N_y = 257$.

RESULTS

Turbulent mean flow and the Reynolds stress

Perturbation	max	λ_x	λ_z
$G_{\max}$	3.31	∞	$4.3h$
$R_{\max}$	11249	∞	$7.4h$
V	157	∞	$5.1h$

Table 1: The maximum amplification by initial perturbation, harmonic forcing and stochastic excitation and the corresponding streamwise and spanwise spacings.

The turbulent mean flow and the associated Reynolds shear stress computed by direct numerical simulation at $Re = 750$ are reported in Fig. 1. To obtain well converged results we have used the same computational box ($L_x \times L_y \times L_z = 28\pi h \times 2h \times 8\pi h$) and resolution ($N_x \times N_y \times N_z = 340 \times 55 \times 170$ after dealiasing) used by Komminaho *et al.* (1996). Re_τ converges to the same $Re_\tau = 52$ found by Komminaho *et al.* (1996) and also shows good agreement with the experimental value $Re_\tau = 50$ reported by Kitoh *et al.* (2005). The mean shear rate at the centreline $d(U/U_w)/d(y/h)|_{y=0} = 0.1865$ is also in good accordance with the 0.18 value found by Komminaho *et al.* (1996) and the experimental value of 0.2. As shown in Fig. 1, the computed mean flow and the associated Reynolds shear stress are almost undistinguishable from from the ones computed by Komminaho *et al.* (1996) and by Tsukahara *et al.* (2005).

Optimal response to initial conditions, harmonic and stochastic forcing

As a preliminary step, the eigenvalues of the Orr-Sommerfeld-Squire operator (4) have been computed and found to be stable. The optimal response to initial condition, harmonic and stochastic forcing have then been computed for a set of wavenumbers α and β, and the main results are summarized in Table 1. The optimal temporal energy growths $G(t, \alpha, \beta)$ are computed allowing the extraction of the respective $G_{max}(\alpha, \beta)$ reported in Fig. 2a. Only elongated structures, roughly the ones with $\alpha < \beta$, are significantly amplified, the most amplified ones being streamwise uniform ($\alpha = 0$ i.e. $\lambda_x = \infty$). The energy growths G_{max} are not very large, attaining a maximum value of 3.31. For streamwise uniform perturbations, the most amplified spanwise wavenumber is $\beta = 1.46/h$ corresponding to the spanwise wavelength $\lambda_z = 4.3h$. As α increases, the most amplified β slightly increases.

The optimal response to harmonic forcing $R(\omega_f, \alpha, \beta)$ is computed for the same set of wavenumbers. A set of forcing frequencies ω_f is considered, and the maximum response $R_{\max}(\alpha, \beta)$ extracted from these data is reported in Fig. 2b. Similarly to the optimal transient growth, only elongated structures are appreciably amplified. For streamwise uniform structures, the largest response ($R_{\max} = 11249$) is obtained for $\beta = 0.85/h$ (corresponding to $\lambda_z = 7.4h$). The dependence of the optimal response on the forcing frequency is shown in Fig. 2c for the most amplified wavenumbers ($\alpha = 0$, $\beta = 0.85/h$). From this figure it is seen that the largest response is obtained when the forcing is steady ($\omega_{f,\max} = 0$) and that the frequency response is strongly concentrated near $\omega_f = 0$. This indicates that the system behaves like a strongly selective low-pass frequency filter.

Finally, the variance $V(\alpha, \beta)$ of the response maintained by the stochastic forcing is computed for the same set of wavenumbers, and it is shown in Fig. 3(a). The selection of elongated structures appears also in this case. The maximum amplification of the variance ($V = 157$) is obtained with streamwise uniform structures and the spanwise

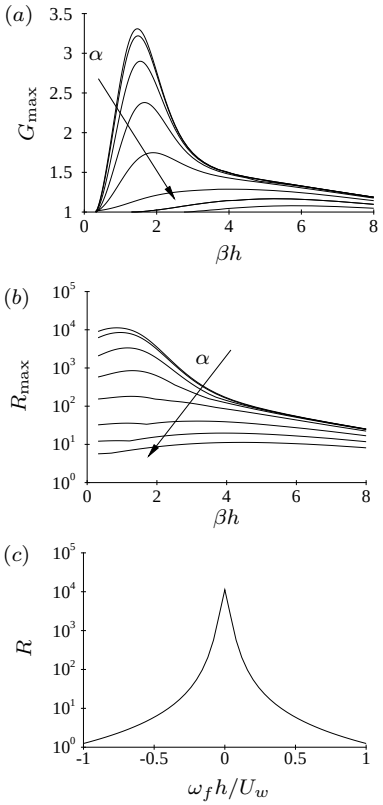

Figure 2: (a) Dependence of the maximum temporal energy growth $G_{\max}$ on the dimensionless spanwise wavenumber βh for selected streamwise wavenumbers (top to bottom: $\alpha h = 0, 0.1, 0.25, 0.5, 1, 2, 3, 4$. (b) Dependence of the maximum energy amplification of harmonic forcing $R_{\max}$ on the dimensionless spanwise wavenumber βh for selected streamwise wavenumbers α (same values as in (a)). (c) Dependence of the optimal energy amplification R on the dimensionless harmonic forcing frequency $\omega_f h/U_w$ for the optimal wavenumbers ($\alpha = 0$,$\beta h = 0.85$).

Flows	Optimal λ_z/h		
	$G_{\max}$	$R_{\max}$	V
Turbulent Couette	$4.3^{(*)}$	$7.4^{(*)}$	$5.1^{(*)}$
Laminar Couette	$3.9^{(a)}$	$5.3^{(a)}$	$4.5^{(b)}$
Turbulent Poiseulle	$4.0^{(c)}$	–	–
Laminar Poiseulle	$3.1^{(a)}$	$3.9^{(a)}$	$3.5^{(b)}$

Table 2: Optimal spanwise wavenumbers of the maximum responses to initial perturbation, harmonic forcing, and stochastic excitation. Results from: (*) the present investigation, (a) Trefethen *et al.* (1992), (b) Jovanović & Bamieh (2005) and (c) Pujals *et al.* (2009)

wavenumber $\beta = 1.23/h$ (corresponding to $\lambda_{z\max} = 5.1h$). The structures with the largest contribution to the variance are then identified using the the Karhunen-Loève decomposition. The twenty largest ratios σ_j/V, representing the contribution of the j-th mode to the total variance, are reported in Fig. 3(b) for the wavenumbers associated to the largest variance (α=0, $\beta = 1.23/h$). We find that the most energetic mode contributes to 79% of the total maintained energy variance, implying that a unique coherent structure strongly dominates the stochastic response in this case.

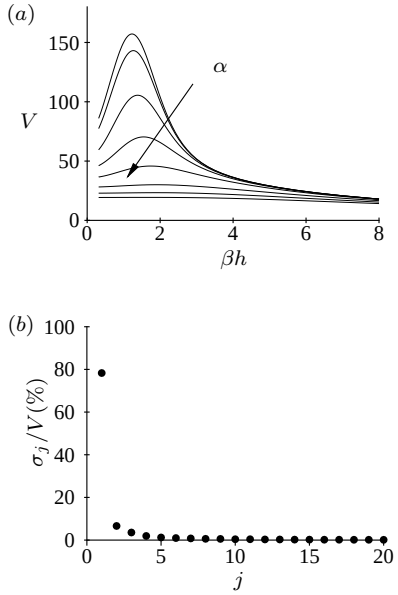

Figure 3: (a) Dependence of the variance V of the response to stochastic forcing on the dimensionless spanwise wavenumber βh for selected streamwise wavenumbers α (same values as in Fig. 2: top to bottom $\alpha h = 0, 0.1, 0.25, 0.5, 1, 2, 3, 4$). (b) Contribution of the leading 20 Karhunen-Loève modes to the total variance.

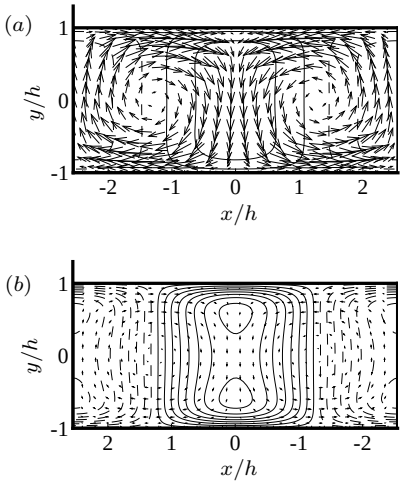

Figure 4: Cross-stream (y-z plane) view of the most energetic forcing (a) and response (b) modes in stochastic forcing. The field corresponds to the optimal wavenumbers $\alpha = 0$ and $\beta h = 1.23$ ($\lambda_z = 5.1h$). Here, the solid and dashed contours denote positive and negative values of the streamwise component respectively (with increment of 0.1 the maximum value of the output) while the cross-stream components are represented as vectors (same scales in input and output plots).

Comparison with previous results

The fact that for all the three types of response, the maximum energy amplification is obtained by streamwise uniform structures ($\alpha = 0$) is in accordance with the similar analyses of other turbulent and laminar flows except possibly only the maximum temporal growth of the laminar Couette flow that is obtained with perturbations non streamwise uniform, but having a very large streamwise wavelength ($\lambda_x = 180h$). The most amplified spanwise wavelength is not the same for the different types of problem: The largest ($\lambda_z = 7.4h$) is found for the harmonic forcing whereas the shortest ($\lambda_z = 4.3h$) is found for the initial value problem, the stochastic forcing one being located in between ($\lambda_z = 5.1h$). The same ordering of spanwise optimal wavelengths is observed for the laminar Couette and Poiseuille flows (see Table 2). Moreover, the spanwise wavelength maximizing G_{max} in the turbulent Couette case is slightly larger than the one found for the laminar case. This is also in accordance with what is observed e.g. for the turbulent Poiseuille flow (as reported in Table 2).

At the very low Reynolds number considered here ($Re_\tau = 52$), the small temporal energy growths that we find ($G_{max} \leq 3.3$) are not surprising if compared e.g. to the turbulent Poiseulle flow case where a maximum growth of the order of 10 is observed for $Re_\tau = 500$ (Pujals *et al.* 2009). The low Reynolds number also explains that the G_{max} curves do not show any sign of the secondary peak associated with near-wall structures with $\lambda_z^+ \approx 90 - 100$, contrary to what is found by del Álamo & Jiménez (2006) and Pujals *et al.* (2009) for the plane Poiseuille flow. In these studies, the secondary peak appeared separated from the primary peak only for sufficiently large Reynolds numbers (typically Re_τ larger than ≈ 300), i.e. when the inner and outer scales are sufficiently separated. The two scales are not separated in the present case ($Re_\tau = 52$) where the expected inner peak value $\lambda_z^+ \approx 100$ corresponds to $\lambda_z \approx 2h$, which is well in the range of the primary peak.

Spatial structure of the optimal input and output perturbations

The spatial structures of optimal perturbations and the corresponding response are also obtained. All these optimals reveal the essentially same physical feature. Therefore, here we only consider the stochastic forcing. In this case, the optimal input (Fig. 4*a*) and output (Fig. 4*b*) are the forcing term and the associated response corresponding to the most energetic Karhunen-Loève mode representing 79% of total variance of the stochastically forced system respectively. Here, note that all the considered outputs most of the energy lies in the streamwise velocity component while for the input field most of the energy is in the cross-stream components. This implies that the dominant physical mechanism for the amplification is the lift-up effect by which streamwise vortices efficiently induce streamwise streaks. This is also in accordance with all the previous results of input-output investigations of laminar and turbulent wall-bounded shear flows.

The wall-normal Fourier components ($\hat{v}$ and $\hat{f}_v$) of the optimal inputs and the streamwise Fourier component ($\hat{u}$) of the optimal outputs shown in Fig. 4 are reported in Fig. 5*a* and *b* respectively. The wall-normal components of the optimal inputs have almost the same shape (Fig. 5*a*). The streak shapes of the corresponding optimal outputs show two maxima at $y/h = \pm 0.66$ for the optimal temporal response, $y/h = \pm 0.59$ for the leading KL mode while the streaks corresponding to the (deterministic) harmonic forcing are almost uniform in the bulk region ($|y/h| \leq 0.5$).

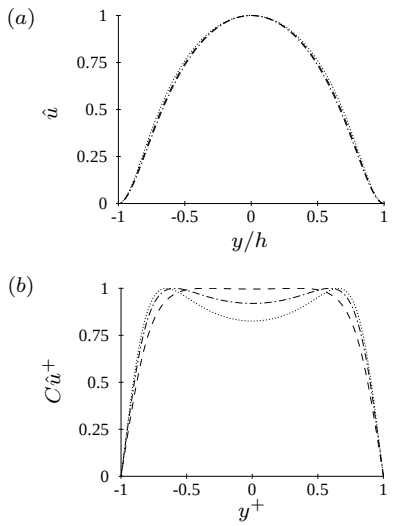

Figure 5: Wall-normal dependence of (*a*) $\hat{v}(y/h), \hat{f}_y(y/h)$ corresponding to the optimal input fields and of (*b*) the streamwise Fourier component $\hat{u}(y/h)$ corresponding to the optimal output velocity fields. In (a) and (b), the maximum values have been normalized to 1 to allow for comparison. Data from the initial value problem (·····) and from the stochastic (—·—·—) and harmonic (- - - -) forcing problems.

DISCUSSION

The scales of the optimal streamwise uniform structures having the largest response to initial conditions ($\lambda_z = 4.3h$) and stochastic forcing ($\lambda_z = 5.1h$) show good agreement with those of the most energetic coherent structures observed in the numerical simulations of Komminaho *et al.* (1996) ($\lambda_z = 4.2h$ and $\lambda_x > 30h$ at $Re = 750$), Tsukahara *et al.* (2006) ($\lambda_z = 4.2 - 5h$ and $\lambda_x \approx 42 - 64h$ at $Re = 750$ and 2150) and in the experiments of Tillmark (1994), Tillmark & Alfredsson (1994) ($\lambda_z \approx 4 - 5h$ and $\lambda_x > 30h$ at $Re = 3300$) and Kitoh & Umeki (2008) ($\lambda_z = 4h$ and $\lambda_x \approx 40 - 60h$ at $Re = 3750$). Furthermore, Tsukahara *et al.* (2006) have found that at $Re = 750$ the most energetic POD modes have scales $\lambda_z = 4.2 - 5.1h$ and $\lambda_x \approx 45h$. This most energetic POD mode shows a striking resemblance with the most energetic mode of the response to stochastic forcing reported in our Fig. 5*b*; the position of the peak in the u response, at $y^+ = 15 - 20$, is also similar.

Our results therefore confirm the strong relation between the optimally amplified streaks and the large-scale coherent streaks measured in experiments and in direct numerical simulations already reported for the turbulent Poiseuille flow (del Álamo & Jiménez 2006; Pujals *et al.* 2009). In all these cases, the observed coherent streaks were not artificially forced, thus it is not surprising that the relevant scales come from the response to stochastic forcing and to initial conditions if one assumes that the effect of the nonlinear terms and of the small-scale fluctuations can be treated either as a stochastic forcing or as random initial conditions. From the viewpoint of flow control and sensitivity to boundary conditions, where the forcing is deterministic and correlated over all times, then, the relevant scales should come from the harmonic forcing analysis. In this case, the present results indicate that the optimal response is obtained with the spanwise spacing $\lambda_z = 7.4h$, larger than the one aris-

ing in the (unforced) observed large-scale coherent streak ($\lambda_z = 4 - 5h$). Furthermore, the very large response to harmonic forcing indicates good controllability of the large-scale structures even at low Reynolds numbers. This extreme sensitivity of the turbulent Couette flow to steady forcing has also been reported by Kitoh *et al.* (2005) and confirmed by Kitoh & Umeki (2008) who artificially forced the large-scale streaks using vortex generators.

CONCLUDING REMARKS

In the present study, we investigate the optimal perturbations in plane turbulent Couette flow at $Re_h = 750$. Direct numerical simulation is conducted to obtain turbulent mean flow and the associated eddy viscosity because no analytical model of the mean flow is available unlike pressure-driven channel flow and boundary layer. The three canonical types of optimal perturbations are computed: the initial optimal perturbations, the response to harmonic forcing and the variance to stochastic excitation. In all the cases, the maximum responses are obtained for streamwise uniform perturbations ($\lambda_x = \infty$). The optimal spanwise spacings of the transient growth and the stochastic forcing are $\lambda_z = 4.2h$ and $\lambda_z = 5.2h$, respectively. These values are in very good agreement with the spanwise spacing of the large-scale streaks reported in previous studies. Moreover, the velocity field of the responses to the optimal perturbations are strikingly similar to that of large-scale structure obtained with direct numerical simulation. Finally, the optimal response to the harmonic forcing, more related to flow controls, reveals the maximum by steady forcing with larger spanwise wavelength ($7.4h$).

The relationship between optimal perturbations and the large-scale outer structure in wall-bounded turbulent flows such as pressure-driven channel and turbulent boundary layer have been successfully investigated by very recent studies. The present findings are further confirmations that this relation also holds in plane turbulent Couette flow. So far, all the investigations have focused only on finding optimal perturbations and their maximal responses with physically proper 'linear' model. Therefore, the resulting nonlinear process such as self-sustaining cycle suggested by e.g. Hamilton *et al.* (1995) should be an subsequent issue. The search for such a self-sustaining cycle of the large-scale coherent structures in turbulent wall-bounded flows and the investigation of the mechanisms selecting their scales are the subject of current intensive investigation.

REFERENCES

del Álamo, J. C., & Jiménez, J. 2006 "Linear energy amplification in turbulent channels", *J. Fluid Mech.*, Vol. 559, p. 205.

Bamieh, B. & Dahleh, M. 2001 "Energy amplification in channel flows with stochastic excitation", *Phys. Fluids*, Vol. 13, p. 3258.

Cossu, C., Pujals, G. & Depardon, S. 2009 "Optimal transient growth and very large scale structures in turbulent boundary layers", *J. Fluid Mech.*, Vol. 619, p. 79.

Farrell, B. F. & Ioannou, P. J. 1993 "Stochastic forcing of the linearized Navier-Stokes equation", *Phys. Fluids A*, Vol. 5, p. 2600.

Gibson, J. F., Halcrow, J., & Cvitanović, P. 2008 Visualizing the geometry of state space in plane Couette flow", *J. Fluid Mech.*, Vol. 611, p. 107. see also http://www.channelflow.org/.

Hamilton, J.M., Kim, J. & Waleffe, F. 1995 "Regeneration mechanisms of near-wall turbulence structures", *J. Fluid Mech*, Vol. 287, p. 317.

Kitoh, O., Nakabayashi, K., & Nishimura, F. 2005 "Experimental study on mean velocity and turbulence characteristics of plane Couette flow, low Reynolds number effects and longitudinal vortical structure", *J. Fluid Mech.*, Vol. 539, p. 199.

Kitoh, O., & Umeki, M. 2008 "Experimental study on large-scale streak structure in the core region of turbulent plane Couette flow", *Phys. Fluids*, Vol. 20, p. 025107.

Komminaho, J., Lundbladh, A., & Johansson, A. V. 1996 "Very large structures in plane turbulent Couette flow", *J. Fluid Mech.*, Vol. 320, p. 259.

Lee, M. J. & Kim, J. 1991 "The structure of turbulence in a simulated plane Couette flow", *Eighth Symp. on Turbulent Shear Flow Tech. University of Munich, Sept. 9-11*, 5.3.1-5.3.6.

Pujals, G., García-Villalva, M., Cossu, C., & Depardon, S. 2008 "A note on optimal transient growth in tutbulent channel flow", *Phys. Fluids*, Vol. 21, p. 015109

Reynolds, W. C. & Hussain, A. K. M. F. 1972 "The mechanics of an organized wave in turbulent shear flow. Part 3. Theoretical models and comparisons with experiments", *J. Fluid Mech.*, Vol. 54 (02), p. 263.

Tillmark, N. 1995 "Experiments on transition and turbulence in plane Couette flow", PhD thesis, Department of Mechanics, Royal Institute of Technology (KTH), S-100 44, Stockholm.

Tillmark, N. & Alfredsson, H. 1994 "Structures in turbulent plane Couette flow obtained from correlation measurements", In *Advances in Turbulences V* (ed. R. Benzi), p. 502. Kluwer.

Jiménez, J. 2007 "Recent developments on wall-bounded turbulence", *Rev. R. Acad. Cien. Serie A Mat.*, Vol. 101, p. 187.

Trefethen, L. N., Trefethen, A. E., Reddy, S. C. & Driscoll, T. A. 1993 "A new direction in hydrodynamic stability: Beyond eigenvalues", *Science*, Vol. 261, p. 578.

Tsukahara, T., Kawamura, H. & Shingai, K. 2006 "DNS of turbulent Couette flow with emphasis on the large-scale structure in the core region", *J. Turbulence.*, Vol. 42.

Tsukahara, T., , Iwamoto, K. & Kawamura, H. 2007 "POD analysis of large-scale structures through DNS of turbulence Couette flow", In *Advances in Turbulence XI.*, p. 245. Porto, Portugal, June 25-28.

Zhou, K., Doyle, J.C. & Glover, K. 1996 *Robust and Optimal Control*. New York: Prentice Hall.